Topological band structure in InAs/GaSb/InAs triple quantum wells

M. Meyer,[1,*] S. Schmid,[1] F. Jabeen,[1] G. Bastard,[2,1] F. Hartmann,[1] and S. Höfling[1,2]

[1]*Technische Physik, Physikalisches Institut and Würzburg-Dresden Cluster of Excellence ct.qmat, Am Hubland, D-97074 Würzburg, Germany*

[2]*Physics Department, École Normale Supérieure, PSL 24 rue Lhomond, 75005 Paris, France*

(Received 22 February 2021; accepted 21 June 2021; published 5 August 2021)

We present gate voltage and temperature dependent transport measurements of InAs/GaSb/InAs triple quantum wells (TQWs) with a designed hybridization gap energy of 4 meV comparable to its traditional double quantum well counterpart. Gate voltage dependent measurements enable us to monitor two electron densities deep in the nonhybridized electron regime and further reveal a clear hybridization gap and a Van Hove singularity in the valence band as a result of the hybridized electron-hole band structure of the TQWs. The evolution of the charge carrier densities and types is studied in detail. Electron and hole densities coexist if the Fermi energy is within the gap and the bottom of the valence band at the Γ point. On the contrary, only single carrier types can be found far in the conduction and valence band. Thus, we are able to identify the topological band structure of these TQWs. Furthermore, the temperature evolution of the hybridized gap of the triple quantum well is studied. We find a rather temperature insensitive hybridization gap energy.

DOI: 10.1103/PhysRevB.104.085301

I. INTRODUCTION

Quantum spin Hall insulators (QSHIs), or two-dimensional topological insulators (2D TIs), are characterized by an insulating bulk and gapless helical edge states [1]. The first experimental observation of these novel classes of materials was on HgTe/CdTe quantum wells back in 2007 [2]. Since then many material systems were proposed to host the QSHI phase such as WTe_2 or Bi_2Se_3 [3–5]. One prominent example is InAs/GaSb double quantum wells (DQW) with their broken band-gap alignment which have been extensively studied in many ways in the literature [6–13]. For the InAs/GaSb DQW the electron and hole states are spatially separated and localized in the InAs and GaSb layers, respectively. This allows control of both the electric field and the Fermi energy (E_F), via a dual gate approach enabling InAs/GaSb DQWs TIs to tune between the trivial and topological phase via externally accessible control parameters [7]. However, the hybridization gap energy in DQWs is much smaller compared to the HgTe/CdTe material system with typical hybridization gaps up to a few millielectron volts only for unstrained and up to 35 meV for highly strained GaSb wells [6,10,14]. Highly strained HgTe/CdTe, for instance, enables gap energies of up to 55 meV [15]. However, elevated temperature operation is hampered by the closing of the hybridization gap at relatively low temperature due to the strong temperature dependence of the Γ6 bulk band in HgCdTe [16,17]. Interestingly, by adding an additional layer of InAs to InAs/GaSb DQWs it is possible to enhance the gap energy up to 60 meV for strained quantum wells albeit profiting from a rather temperature insensitive hybridization gap energy [18]. The additional InAs layer eliminates the structure inversion asymmetry (in ideal structures). The phase diagram with its bulk insulating phase, its TI phase, and its semimetallic phase is accessible via thickness control of the InAs and GaSb quantum well thicknesses, comparable to the phase diagram of HgTe/CdTe. In addition, other interesting phases such as the bilayer graphene phase [for GaSb/InAs/GaSb triple quantum wells (TQWs)] should emerge [18]. Up to now, only a few experimental realizations of TQWs with an inverted band structure have been reported in the literature. In 2018, Krishtopenko *et al.* measured the interband optical transitions by Landau-level spectroscopy and extracted the gap energy out of terahertz photoluminescence at different temperatures [19]. Their experimental results support that the gap is temperature independent. Also they report evidence for a gapless state in their sample and therefore massless Dirac fermions by magnetotransport measurements [20].

In this study, we present electronic transport measurements of an InAs/GaSb/InAs TQW with designed hybridization gap energies comparable to traditional DQWs and demonstrate the topological band structure in InAs/GaSb/InAs triple quantum wells. By tuning with a single top-gate voltage (V_{TG}), the charge carrier densities and types can be monitored and correlated to the hybridized and nonhybridized band structure. Magnetotransport measurements with a top gate reveal two distinct frequencies in the Shubnikov–de Haas (SdH) oscillations, associated with different electron charge carrier densities in the two InAs quantum wells. At the middle of the hybridization gap, a maximum is measured in the longitudinal resistance R_{xx}. At this point electron and hole concentrations coincide and therefore it is called the charge neutrality point (CNP). We find that coexisting electron and hole carrier densities occur within the narrow energy range between the CNP and the hybridized valence band. Furthermore, we study the temperature evolution of the hybridization gap energy.

*manuel.meyer@physik.uni-wuerzburg.de

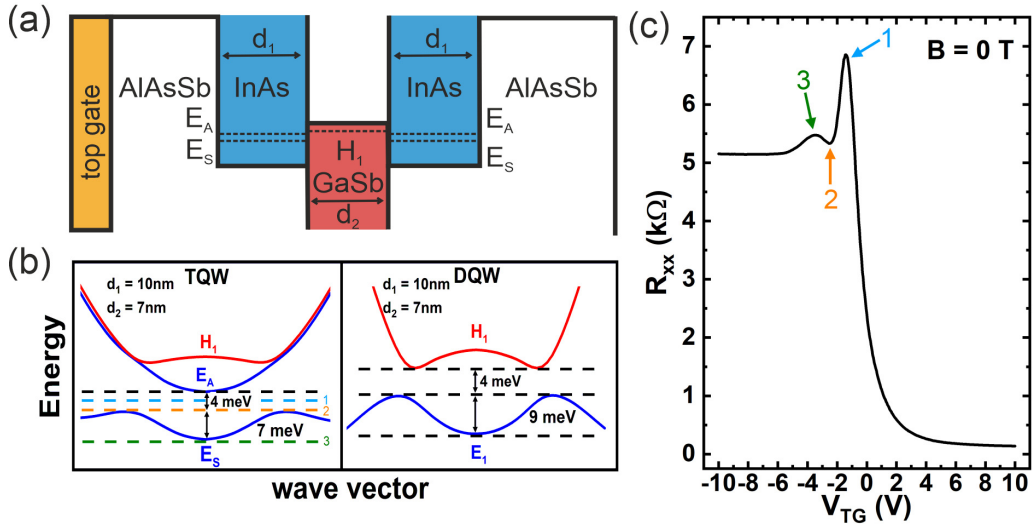

FIG. 1. (a) Schematic band structure of the InAs/GaSb/InAs TQW embedded in $AlAs_{0.08}Sb_{0.92}$ barriers. Both InAs wells have equal thicknesses d_1 and the GaSb well thickness d_2. Due to tunnel coupling of both InAs wells the E_1 level splits into two energy levels, E_A and E_S (for antisymmetric and symmetric).The top gate is used to tune the charge carrier density from an electron dominated regime to a hole dominated regime over the topological insulating band gap. (b) Simulated band dispersion relation for the sample under study (TQW) compared to a DQW with equal InAs well width $d_1 = 10$ nm and GaSb well width $d_2 = 7$ nm. The hybridization gap energies are comparable, e.g., around 4 meV. The energy difference between the top of the valence band and the local minimum is approximately 7 and 9 meV for the TQW and DQW, respectively. (c) Gate voltage trace of the longitudinal resistance R_{xx} at $T = 4$ K and $B = 0$ T for the TQW. The colored arrows mark the corresponding position of the Fermi energy E_F in panel (b) (color-coded dashed lines).

II. RESULTS AND DISCUSSION

A schematic band profile of a TQW is shown in Fig. 1(a). The TQW is composed of two InAs wells with (symmetrical) thickness d_1 which surround a single GaSb well with thickness d_2. The TQW is embedded in either AlSb barriers or AlAsSb barriers (the later one is used in this study and with $AlAs_{0.08}Sb_{0.92}$ lattice matched to GaSb). Via a top gate, the electric field and Fermi energy can be tuned. Due to the broken band-gap alignment, the electron and hole states are spatially separated in the InAs and GaSb layers, respectively [21]. The second InAs quantum well restores inversion symmetry and the hybridization gap in the TQWs can open at $k = 0$. Due to the tunnel coupling, the electron level splits into an antisymmetrical (E_A) and a symmetrical (E_S) part [18]. Figure 1(b) shows numerically simulated dispersion relations, performed via the NEXTNANO simulation tool, for the TQW (left-hand side) and a DQW (right-hand side) with thicknesses $d_1 = 10$ nm and $d_2 = 7$ nm [22]. Although the hybridization gap energy E_{gap} in the TQW can be designed in a broad range, we aimed to design a TQW with hybridization gap energy similar to a DQW, i.e., 4 meV. Thus, the thicknesses of $d_1 = 10$ nm and $d_2 = 7$ nm were chosen. In addition, the difference between the top of the valence band and the local minimum at the Γ point are comparable with 7 meV for the TQW and 9 meV for the DQW. For both simulated structures, the electron and hole subbands are crossing away from the Γ point at a finite k_{cross} [18]. One important difference is that for this TQW the indirect gap is between the E_A and E_S levels, whereas for the DQW the hybridization gap is between the H_1 and E_1 levels.

Our heterostructure was grown by molecular beam epitaxy (MBE). A 200 nm undoped GaSb buffer was first grown on a GaSb substrate, followed by a 10 × 2.5/2.5 nm GaSb/AlSb superlattice. On top of the superlattice the InAs/GaSb/InAs (10/7/10 nm) TQW is sandwiched between a 100 nm thick $AlAs_{0.08}Sb_{0.92}$ bottom barrier and a 50 nm thick $AlAs_{0.08}Sb_{0.92}$ top barrier. The sample is terminated by a 3 nm thick GaSb cap. After the growth, Hall bars were fabricated. The length and width of the studied Hall bar are 60 and 20 μm, respectively. The top gate consists of 30 nm Cr/100 nm Au and is separated from the heterostructure with a 5 × 10/10 nm SiO_2/Si_3N_4 superlattice. All measurements were performed in the dark and, if not stated otherwise, at $T = 4.2$ K. Note that due to different cooling cycles and charged deep traps (because of the top gate) there are small hysteresis effects between the different measurements. This results, for example, in a slight shift of the CNP [23].

Figure 1(c) shows R_{xx} as a function of V_{TG} from +10 V to −10 V at zero magnetic field. R_{xx} is lowest at $V_{TG} = +10$ V with a value of around 30 Ω due to the high mobility deep in the electron regime. For decreasing V_{TG}, the resistance increases and peaks at around $V_{TG} = -1.5$ V with a value of ∼7 kΩ. This value is below $h/2e^2 = 12.9$ kΩ because of residual bulk conductivity and trivial edge channels [23–25]. After the resistance peak a local minimum is reached (at $V_{TG} \approx -2.5$ V), followed by a local maximum (at $V_{TG} \approx -3.5$ V). For lower V_{TG}, the resistance saturates at around 5.2 kΩ. This results from a constant charge carrier density of the holes which probably results from a Fermi level pinning in the valence band (VB). However, the origin of this pinning is not completely clear. Certain points in R_{xx} are marked which correspond to characteristic Fermi energy positions as illustrated in the dispersion relation [Fig. 1(b) left side]: Point 1 (light blue) is the resistance peak and the middle of the hybridization gap. Point 2 (orange) is the local minimum in R_{xx} and the top

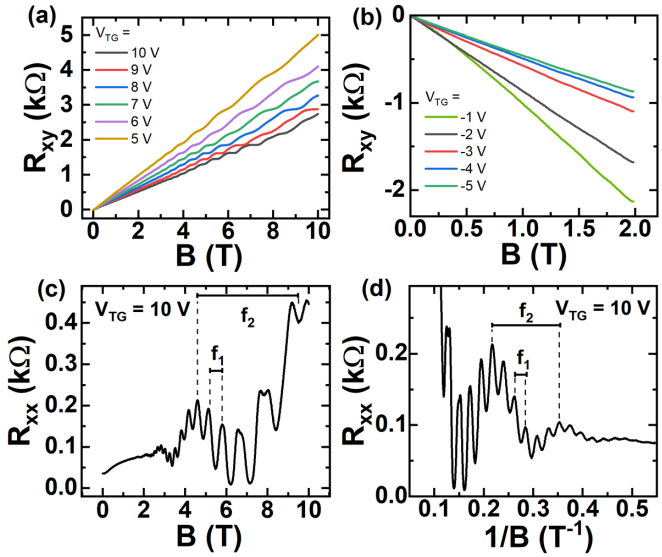

FIG. 2. (a) Hall resistance as a function of the magnetic field $B = 0$–10 T and $V_{TG} = +10$ to $+5$ V (deep in the electron regime) and in (b) for $B = 0$–2 T and $V_{TG} = -1$ to -5 V. In the electron and hole regime the slope is linear, whereas a weak nonlinearity can be seen for the Hall trace within the hybridization gap, e.g., as depicted for $V_{TG} = -1$ and -2 V, due to the coexistence of electrons and holes. (c) SdH oscillations over B and (d) $1/B$ for $V_{TG} = 10$ V. From the oscillations, two frequencies f_1 and f_2 can be extracted due to different charge carrier densities in the upper and lower InAs well, respectively.

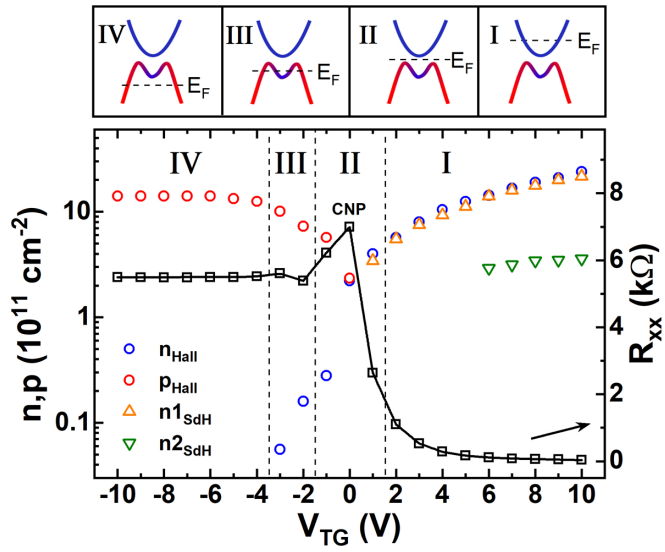

FIG. 3. Electron and hole charge carrier densities for different regions I–IV (corresponds to E_F at certain points in the dispersion relation), as extracted by the two-carrier fitting (blue and red circles). In region I, only electrons exist. Between $V_{TG} = 10$ and 6 V, two prominent frequencies appear in the SdH oscillations [Figs. 2(c) and 2(d)] caused by different charge carrier densities in the upper and lower InAs well. From these frequencies, the densities $n1_{SdH}$ and $n2_{SdH}$ are extracted (orange and green triangles). For $V_{TG} < 6$ V, $n2_{SdH}$ vanishes. By further decreasing V_{TG}, the Fermi energy enters the hybridization gap (region II). At $V_{TG} = 0$ V (CNP) a hole density appears. In region III, E_F lies in the hybridized part of the VB where a minor charge density of electrons (around 10^{10} cm^{-2}) coexists while holes are now the majority charge carriers. By further decreasing V_{TG}, the electron density vanishes completely and only holes exist (region IV). For comparison R_{xx} for $B = 0$ T (in black) is also depicted.

of the valence band, the so-called Van Hove singularity (VHS) [26–28]. Point 3 (green) is the local maximum in R_{xx} and the local minimum in the VB. Note that for this particular TQW, where the hybridization gap lies between E_A and E_S, only the VHS in the valence band is visible in R_{xx} as can be seen in the measurement. In comparison for DQWs with a hybridized band structure a dip in R_{xx} on both sides of the gap should be visible corresponding to the VHS in the conduction band (CB) and VB [7,26].

Figure 2(a) provides exemplary Hall measurements for magnetic fields up to 10 T and positive gate voltages $V_{TG} =$ 5–10 V. The Hall resistances R_{xy} are linear at low magnetic fields and quantum Hall plateaus at even fractions of $h/2e^2$ ($h =$ Planck constant, $e =$ elementary charge) emerge. At larger magnetic fields, the spin degeneracy is lifted and plateaus are indicated at integer fractions of h/e^2 [24]. No quantum Hall plateaus are visible for gate voltages below $V_{TG} = +1$ V.

Figure 2(b) shows the Hall traces for $V_{TG} = -1$ V to -5 V. For negative V_{TG}, R_{xy} is nonlinear until $V_{TG} = -3$ V and finally evolves linearly for lower gate voltages. The nonlinearity of the Hall traces for $V_{TG} = -1$ to -3 V occurs due to the coexisting electron and hole populations within this gate voltage range. To accurately determine the respective charge carrier densities, a two-carrier fitting is required [7] (see Supplemental Material [29]). The longitudinal resistance R_{xx} for $V_{TG} = +10$ V is shown in Figs. 2(c) and 2(d) as a function of B and $1/B$, respectively. Clear SdH oscillations with two distinct frequencies f_1 and f_2 are visible due to different charge carrier densities in both InAs wells.

Figure 3 shows all the acquired charge carrier densities (out of the Hall resistance and SdH oscillations) as a function of the gate voltage V_{TG}. As a comparison, the longitudinal resistance R_{xx} for $B = 0$ T is plotted as black solid rectangles. The schemes at the top of Fig. 3 show where E_F lies in the dispersion relation for different gate voltage ranges. Note that these schemes are simplified and just for illustration. They do not consider the gate induced asymmetry which will change the dispersion relation significantly for really high positive/negative V_{TG}.

For $V_{TG} = 10$–1 V, E_F lies in the CB (region I). These high gate voltages weaken the tunnel coupling between both InAs wells, leading to two independent InAs wells with charge carrier densities $n1_{SdH}$ (orange triangles) and $n2_{SdH}$ (green triangles). Both densities have a maximum value of $n1_{SdH,max} = 2 \times 10^{12}$ cm^{-2} and $n2_{SdH,max} = 3 \times 10^{11}$ cm^{-2} and they correspond to the upper and lower InAs well, respectively. The large difference results from stronger tuning of the upper well than the lower well. With the difference of both densities Δn the energy difference between both wells is determined at $V_{TG} = 10$ V : $\Delta E = \frac{\pi\hbar^2}{m_e}\Delta n \approx 92$ meV. Here, $m_e = 0.04$ is the effective mass of electrons (in units of free electron mass) [19]. In addition, if a linear fit is applied to $n1_{SdH}$ and $n2_{SdH}$ the charge carrier density at the CNP can be extracted: $n1_{SdH} = n2_{SdH} = 1.3 \times 10^{11}$ cm^{-2}. For $V_{TG} < 6$ V f_2 vanishes

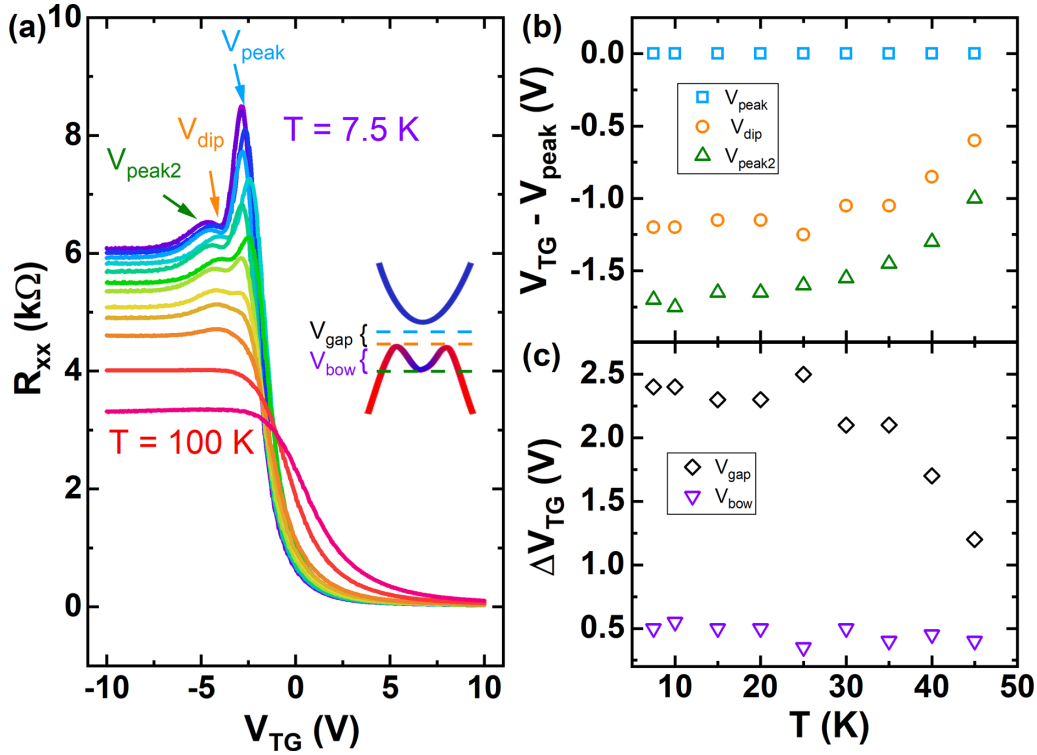

FIG. 4. (a) Temperature dependent resistance for $V_{\mathrm{TG}} = +10\,\mathrm{V}$ to $-10\,\mathrm{V}$. With increasing temperature the resistance peak corresponding to the hybridization gap reduces until it completely vanishes for $T = 50\,\mathrm{K}$ (yellow curve) which corresponds to $E_{\mathrm{gap}} = k_{\mathrm{B}}T \approx 4.3\,\mathrm{meV}$. This indicates a rather temperature insensitive hybridization gap. The inset shows a scheme of the band structure with certain positions. (b) Position of V_{peak}, V_{dip}, and V_{peak2} normalized to V_{peak}. The difference between V_{dip} or V_{peak2} and V_{peak} is decreasing whereas the difference between V_{dip} and V_{peak2} is staying nearly equal. This can also be seen in (c), where the voltage difference for the gap (V_{gap}) and for the bowing (V_{bow}) is shown. V_{gap} decreases whereas V_{bow} is nearly constant.

and $n2_{\mathrm{SdH}}$ cannot be extracted anymore. The blue and red circles are the complete charge carrier densities for electrons and holes extracted from fitting the Hall traces. At $V_{\mathrm{TG}} = 10\,\mathrm{V}$ a maximum electron density of $n_{\mathrm{Hall,max}} = 2.4 \times 10^{12}\,\mathrm{cm}^{-2}$ with a maximum mobility of $\mu_{\mathrm{max}} = 2.2 \times 10^{5}\,\mathrm{cm}^2/\mathrm{V\,s}$ is reached. This value is a factor—two to three times lower than the highest mobility values for DQWs reported in the literature [24,30]. By decreasing V_{TG}, n_{Hall} decreases linearly. Around $V_{\mathrm{TG}} = 1\,\mathrm{V}$ a transition to the hybridization gap (region II) is made. At $V_{\mathrm{TG}} = 0\,\mathrm{V}$, the charge neutrality point (CNP), a hole density appears. At this point both charge carrier densities are nearly equal with $n_{\mathrm{CNP}} \approx p_{\mathrm{CNP}} \approx 2.2 \times 10^{11}\,\mathrm{cm}^{-2}$. With these values the crossing of the electron and hole bands is calculated to $k_{\mathrm{cross}} \approx 0.12 \times 10^{9}\,\mathrm{m}^{-1}$ which is consistent with the simulations. Also the value for k_{cross} is similar compared to values for the DQWs from the literature [7,31].

In region III, E_{F} lies in the hybridized part of the VB. Here, holes coexist with a minority of electrons of approximately $10^{11}\,\mathrm{cm}^{-2}$ density. By further decreasing V_{TG}, E_{F} lies deep in the VB. The electron density vanishes and the hole density increases until it saturates at a maximum value of $p_{\mathrm{Hall,max}} = 1.41 \times 10^{12}\,\mathrm{cm}^{-2}$ and a mobility of $\mu_{\mathrm{p}} = 2.5 \times 10^{3}\,\mathrm{cm}^2/\mathrm{V\,s}$ (region IV).

The hybridization gap energy E_{gap} is determined via the position of the middle of the gap (V_{peak}) and the VHS (V_{dip}) [27,31,32]: $E_{\mathrm{gap}} = 2(V_{\mathrm{peak}} - V_{\mathrm{dip}})\frac{\Delta p}{\Delta V}\frac{1}{\mathrm{DOS}} =$ 3.2 meV. Here, $\frac{\Delta p}{\Delta V} = \frac{\Delta n}{\Delta V} = 2.4 \times 10^{11}\,\mathrm{cm}^{-2}$ is the linear change of the charge carrier density with V_{TG} and the DOS $= (\mathrm{m_e} + m_h)/\pi\hbar^2$ is the combined density of states for electrons and holes with $m_e = 0.04$ and $m_h = 0.35$ (in units of free electron mass) [19,33]. The value of the experimentally derived hybridization gap of 3.2 meV is slightly smaller than the one extracted from the simulations (4 meV) which could be due to quantum level broadening [7], though this equation just gives an estimate of the hybridization gap but is used throughout the literature. This allows us to compare the different systems (DQW and TQW) with each other.

The band ordering of the Γ6 and Γ8 bands in InAs, GaSb, and AlSb should be temperature insensitive which could enable a temperature independent hybridization gap in comparison to HgTe/CdTe [18,19,34]. Therefore, temperature dependent measurements were performed on the sample. In Fig. 4(a) R_{xx} is shown from $V_{\mathrm{TG}} = +10$ to $-10\,\mathrm{V}$ for temperatures from 8 K up to 100 K. We would like to note that this temperature series was carried out at another but nominally identical sample (same process and dimension, similar charge carrier density and mobility). For increasing temperatures, the resistance in the electron regime increases while the gap resistance value and the hole region resistance value are decreasing. The decrease of the gap resistance value shows the insulating character [11]. The resistance peak at position V_{peak} vanishes for temperatures at around 50 K (yellow curve). This allows to estimate a gap energy of $E_{\mathrm{gap}} =$

4.3 meV which is consistent with the simulated gap value of around 4 meV at $T = 4$ K. Again, this technique is just indicative for the size of the hybridization gap, though the second peak (V_{peak2}, resulting from the hybridized band structure [26]) is still observable but ultimately vanishes at even higher temperatures, i.e., around $T = 100$ K. Figure 4(b) shows the extracted voltage positions of the middle of the hybridization gap (V_{peak}), the valence band maximum (V_{dip}), and the local minimum of the valence band (V_{peak2}). All voltage values are referred to V_{peak}. The voltage differences between V_{peak} and V_{dip} ($V_{gap}/2$) is proportional to the gap energy, i.e., via $E_{gap} = 2(V_{peak}-V_{dip})\frac{\Delta p}{\Delta V}\frac{1}{DOS}$. The voltage difference between V_{dip} and V_{peak2} (which is named V_{bow}) on the other hand is proportional to the energy difference from the top of the VB and the local minimum in the VB at the Γ point. V_{gap} and V_{bow} as a function of temperature are shown in Fig. 4(c).

For increasing temperatures, V_{gap} is decreasing whereas V_{bow} remains nearly constant. This could indicate that the gap is closing but the bowing remains constant. From simulations, though, a gap closing is always accompanied by variations of the bowing in the VB. Hence, those results seem at first glance contradictory but may point to insufficiently known band parameters. However, we would like to note that thermally activated charge carriers will significantly contribute to the exact energy position of V_{peak} and V_{dip} (and therefore V_{gap}) while for V_{peak2} in the VB the charge carrier density is expected to be rather temperature insensitive. Therefore, the nearly constant value for V_{bow} seems more plausible than the decreasing value for V_{gap}. All these experimental indications point to a rather temperature insensitive hybridization gap in this measured temperature region as assumed in the literature [18,19].

III. CONCLUSION

In summary, we have presented gate voltage dependent and temperature dependent transport measurements of a symmetrically grown InAs/GaSb/InAs TQW with a designed hybridization gap energy comparable to its traditional double quantum well counterpart. We observed a clear charge neutrality point in the hybridization gap and a Van Hove singularity in the valence band of the TQW due to the hybridized electron-hole band structure. The evolution of the charge carrier density and type was studied in detail. Electron and hole densities coexist within the CNP and the bottom of the valence band at the Γ point. Deep in the conduction and valence band, only a single carrier type could be found. Thus, we have been able to identify the topological band structure of these TQWs. The temperature evolution of the hybridization gap energy of the triple quantum well was studied. We find that the resistance peak for the hybridization gap vanishes at a temperature of 50 K which corresponds to an energy of $E_{gap} =$ 4.3 meV. This indicates a rather temperature insensitive hybridization gap since the gap energy at $T = 4$ K is found to be about 4 meV. If this temperature insensitivity is also found for higher hybridization gap energies at a broad temperature range it could enable operations at elevated temperatures for InAs/GaSb/InAs TQWs.

ACKNOWLEDGMENTS

The work was supported by the Elite Network of Bavaria within the graduate program "Topological Insulators." Expert technical assistance by A. Wolf and M. Emmerling is gratefully acknowledged.

[1] B. A. Bernevig, T. L. Hughes, and S. C. Zhang, Quantum spin Hall effect and topological phase transition in HgTe quantum wells, Science **314**, 1757 (2006).

[2] M. König, L. W. Molenkamp, X. Qi, and S. Zhang, Quantum spin Hall insulator state in HgTe quantum wells, Science **318**, 766 (2007).

[3] S. Wu, V. Fatemi, Q. D. Gibson, K. Watanabe, T. Taniguchi, R. J. Cava, and P. Jarillo-Herrero, Observation of the quantum spin Hall effect up to 100 Kelvin in a monolayer crystal, Science **359**, 76 (2018).

[4] Y. Xia, D. Qian, D. Hsieh, L. Wray, A. Pal, H. Lin, A. Bansil, D. Grauer, Y. S. Hor, R. J. Cava, and M. Z. Hasan, Observation of a large-gap topological-insulator class with a single Dirac cone on the surface, Nat. Phys. **5**, 398 (2009).

[5] H. Zhang, C. X. Liu, X. L. Qi, X. Dai, Z. Fang, and S. C. Zhang, Topological insulators in Bi_2Se_3, Bi_2Te_3 and Sb_2Te_3 with a single Dirac cone on the surface, Nat. Phys. **5**, 438 (2009).

[6] C. Liu, T. L. Hughes, X.-L. Qi, K. Wang, and S.-C. Zhang, Quantum Spin Hall Effect in Inverted Type-II Semiconductors, Phys. Rev. Lett. **100**, 236601 (2008).

[7] F. Qu, A. J. A. Beukman, S. Nadj-Perge, M. Wimmer, B.-M. Nguyen, W. Yi, J. Thorp, M. Sokolich, A. A. Kiselev, M. J. Manfra, C. M. Marcus, and L. P. Kouwenhoven, Electric and Magnetic Tuning between the Trivial and Topological Phases in InAs/GaSb Double Quantum Wells, Phys. Rev. Lett. **115**, 036803 (2015).

[8] F. Nichele, A. N. Pal, P. Pietsch, T. Ihn, K. Ensslin, C. Charpentier, and W. Wegscheider, Insulating State and Giant Nonlocal Response in an InAs/GaSb Quantum Well in the Quantum Hall Regime, Phys. Rev. Lett. **112**, 036802 (2014).

[9] M. Karalic, C. Mittag, S. Mueller, T. Tschirky, W. Wegscheider, K. Ensslin, T. Ihn, and L. Glazman, Phase slips and parity jumps in quantum oscillations of inverted InAs/GaSb quantum wells, Phys. Rev. B **99**, 201402(R) (2019).

[10] L. Du, T. Li, W. Lou, X. Wu, X. Liu, Z. Han, C. Zhang, G. Sullivan, A. Ikhlassi, K. Chang, and R.-R. Du, Tuning Edge States in Strained-Layer InAs/GaInSb Quantum Spin Hall Insulators, Phys. Rev. Lett. **119**, 056803 (2017).

[11] I. Knez, R. R. Du, and G. Sullivan, Finite conductivity in mesoscopic Hall bars of inverted InAs/GaSb quantum wells, Phys. Rev. B **81**, 201301(R) (2010).

[12] V. S. Pribiag, A. J. A. Beukman, F. Qu, M. C. Cassidy, C. Charpentier, W. Wegscheider, and L. P. Kouwenhoven, Edge-mode superconductivity in a two-dimensional topological insulator, Nat. Nanotechnol. **10**, 593 (2015).

[13] E. M. Spanton, K. C. Nowack, L. Du, G. Sullivan, R.-R. Du, and K. A. Moler, Images of Edge Current in InAs/GaSb Quantum Wells, Phys. Rev. Lett. **113**, 026804 (2014).

[14] H. Irie, T. Akiho, F. Couëdo, K. Suzuki, K. Onomitsu, and K. Muraki, Energy gap tuning and gate-controlled topological phase transition in InAs/$In_xGa_{1-x}Sb$ composite quantum wells, Phys. Rev. Mater. **4**, 104201 (2020).

[15] P. Leubner, L. Lunczer, C. Brüne, H. Buhmann, and L. W. Molenkamp, Strain Engineering of the Band Gap of HgTe Quantum Wells Using Superlattice Virtual Substrates, Phys. Rev. Lett. **117**, 086403 (2016).

[16] S. Wiedmann, A. Jost, C. Thienel, C. Brüne, P. Leubner, H. Buhmann, L. W. Molenkamp, J. C. Maan, and U. Zeitler, Temperature-driven transition from a semiconductor to a topological insulator, Phys. Rev. B **91**, 205311 (2015).

[17] M. Marcinkiewicz, S. Ruffenach, S. S. Krishtopenko, A. M. Kadykov, C. Consejo, D. B. But, W. Desrat, W. Knap, J. Torres, A. V. Ikonnikov, K. E. Spirin, S. V. Morozov, V. I. Gavrilenko, N. N. Mikhailov, S. A. Dvoretskii, and F. Teppe, Temperature-driven single-valley Dirac fermions in HgTe quantum wells, Phys. Rev. B **96**, 035405 (2017).

[18] S. S. Krishtopenko and F. Teppe, Quantum spin Hall insulator with a large bandgap, Dirac fermions, and bilayer graphene analog, Sci. Adv. **4**, eaap7529 (2018).

[19] S. S. Krishtopenko, S. Ruffenach, F. Gonzalez-Posada, G. Boissier, M. Marcinkiewicz, M. A. Fadeev, A. M. Kadykov, V. V. Rumyantsev, S. V. Morozov, V. I. Gavrilenko, C. Consejo, W. Desrat, B. Jouault, W. Knap, E. Tournié, and F. Teppe, Temperature-dependent terahertz spectroscopy of inverted-band three-layer InAs/GaSb/InAs quantum well, Phys. Rev. B **97**, 245419 (2018).

[20] S. S. Krishtopenko, W. Desrat, K. E. Spirin, C. Consejo, S. Ruffenach, F. Gonzalez-Posada, B. Jouault, W. Knap, K. V. Maremyanin, V. I. Gavrilenko, G. Boissier, J. Torres, M. Zaknoune, E. Tournié, and F. Teppe, Massless Dirac fermions in III-V semiconductor quantum wells, Phys. Rev. B **99**, 121405(R) (2019).

[21] H. Kroemer, The 6.1 Å family (InAs, GaSb, AlSb) and its heterostructures: A selective review, Phys. E (Amsterdam, Neth.) **20**, 196 (2004).

[22] See https://www.nextnano.de/index.php for NEXTNANO.

[23] S. Mueller, C. Mittag, T. Tschirky, C. Charpentier, W. Wegscheider, K. Ensslin, and T. Ihn, Edge transport in InAs and InAs/GaSb quantum wells, Phys. Rev. B **96**, 075406 (2017).

[24] B. M. Nguyen, A. A. Kiselev, R. Noah, W. Yi, F. Qu, A. J. A. Beukman, F. K. De Vries, J. Van Veen, S. Nadj-Perge, L. P. Kouwenhoven, M. Kjaergaard, H. J. Suominen, F. Nichele, C. M. Marcus, M. J. Manfra, and M. Sokolich, Decoupling Edge versus Bulk Conductance in the Trivial Regime of an InAs/GaSb Double Quantum Well Using Corbino Ring Geometry, Phys. Rev. Lett. **117**, 077701 (2016).

[25] L. Du, I. Knez, G. Sullivan, and R.-R. Du, Robust Helical Edge Transport in Gated InAs/GaSb Bilayers, Phys. Rev. Lett. **114**, 096802 (2015).

[26] M. Karalic, S. Mueller, C. Mittag, K. Pakrouski, Q. Wu, A. A. Soluyanov, M. Troyer, T. Tschirky, W. Wegscheider, K. Ensslin, and T. Ihn, Experimental signatures of the inverted phase in InAs/GaSb coupled quantum wells, Phys. Rev. B **94**, 241402(R) (2016).

[27] M. J. Yang, C. H. Yang, B. R. Bennett, and B. V. Shanabrook, Evidence of a Hybridization Gap in "Semimetallic" InAs/GaSb Systems, Phys. Rev. Lett. **78**, 4613 (1997).

[28] I. Brihuega, P. Mallet, H. González-Herrero, G. Trambly De Laissardière, M. M. Ugeda, L. Magaud, J. M. Gómez-Rodríguez, F. Ynduráin, and J. Y. Veuillen, Unraveling the Intrinsic and Robust Nature of Van Hove Singularities in Twisted Bilayer Graphene by Scanning Tunneling Microscopy and Theoretical Analysis, Phys. Rev. Lett. **109**, 196802 (2012).

[29] See Supplemental Material at http://link.aps.org/supplemental/10.1103/PhysRevB.104.085301 for details on the two carrier fit.

[30] B. M. Nguyen, W. Yi, R. Noah, J. Thorp, and M. Sokolich, High mobility back-gated InAs/GaSb double quantum well grown on GaSb substrate, Appl. Phys. Lett. **106**, 032107 (2015).

[31] I. Knez, R.-R. Du, and G. Sullivan, Evidence for Helical Edge Modes in Inverted InAs/GaSb Quantum Wells, Phys. Rev. Lett. **107**, 136603 (2011).

[32] M. Altarelli, Electronic structure and semiconductor-semimetal transition in InAs-GaSb superlattices, Phys. Rev. B **28**, 842 (1983).

[33] L. S. Kim, H. D. Drew, H. Munekata, L. L. Chang, and L. Esaki, Electron and hole cyclotron resonance in semimetallic GaSb/InAs/GaSb quantum wells, Solid State Commun. **66**, 873 (1988).

[34] S. Krishnamurthy, A. B. Chen, A. Sher, and M. Van Schilfgaarde, Temperature dependence of band gaps in HgCdTe and other semiconductors, J. Electron. Mater. **24**, 1121 (1995).